The low-temperature magnetic and thermal properties and electronic structure of CeAgAl; experiment and calculations

2008 J. Phys.: Condens. Matter 20 315208

(http://iopscience.iop.org/0953-8984/20/31/315208)

J. Phys.: Condens. Matter **20** (2008) 315208 (8pp) doi:10.1088/0953-8984/20/31/315208

The low-temperature magnetic and thermal properties and electronic structure of CeAgAl; experiment and calculations

A Ślebarski[1,3], D Kaczorowski[2], W Głogowski[1] and J Goraus[1]

[1] Institute of Physics, University of Silesia, Uniwersytecka 4, 40-007 Katowice, Poland
[2] Institute of Low Temperature and Structure Research, Polish Academy of Sciences, PO Box 1410, 50-950 Wrocław, Poland

E-mail: andrzej.slebarski@us.edu.pl

Received 6 March 2008, in final form 30 May 2008
Published 17 July 2008
Online at stacks.iop.org/JPhysCM/20/315208

Abstract

CeAgAl has been known as an orthorhombic system of the $CeCu_2$-type with inhomogeneous magnetic ground state. We report here measurements of the magnetic susceptibility, specific heat and electrical resistivity of this compound, which all displayed low-temperature anomalies attributable to a Kondo ferromagnet. Our XPS studies revealed the presence of stable Ce^{3+} ions and rather weak hybridization of the $4f^1$ states with the conduction band. Moreover, the electronic structure of CeAgAl was studied by means of linearized muffin-tin orbitals (LMTO) and full potential linear augmented plane waves (LAPW) calculations. Both approaches yielded a magnetic ground state, and the Ce magnetic moment calculated by the LAPW method is $\sim 0.9\ \mu_B$, in good agreement with the experimental data. Analysis of both the experimental and calculated results suggests random distribution of the Ag and Al atoms on a single position in the crystallographic unit cell.

(Some figures in this article are in colour only in the electronic version)

1. Introduction

Heavy-electron (HF) behavior found in a number of Ce-based compounds has attracted a great deal of attention [1, 2] and even now it is being studied extensively. Heavy fermions are physical realizations of the Landau concept of a Fermi liquid (for a recent review see [3]) due to the effect of strong interactions among quasi-particles. The physics of heavy fermions is essentially due to the combined action of the Kondo effect, with a tendency to screen magnetic moments and hence produce a non-magnetic ground state, and the RKKY interaction, which favors long-range magnetic ordering. Thus, the behavior of a Kondo lattice is governed by two energy scales: the Kondo temperature $T_K \sim \exp(-1/|J_{fs}N(\epsilon_F|)$ and the RKKY interaction temperature $T_{RKKY} \sim J_{fs}^2 N(\epsilon_F)$, where J_{fs} represents the strength of the exchange interaction between f electrons and conduction electrons and $N(\epsilon_F)$ is the density of states (DOS) at the Fermi level. For Ce-based compounds such an interplay of these two phenomena directly leads to the Doniach phase diagram [4]. For small values of $J_{fs}N(\epsilon_F)$ there is a long-range ordered magnetic phase in the diagram, being in general antiferromagnetic (AF). For large values of $J_{fs}N(\epsilon_F)$ a non-magnetic HF ground state is formed. Most interestingly, the Doniach diagram displays a quantum critical point (QCP), which occurs at the critical value of $J_{fs}N(\epsilon_F)$ at which the magnetic phase becomes unstable.

The stability of the paramagnetic versus the magnetic ground state in a Kondo lattice is strongly dependent on the on-site hybridization energy among conduction and f electrons, V, the bare f-level position in the conduction band, E_f, the magnitude of intrasite Coulomb interaction between two f electrons with opposite spins, U, and the number of electrons per atom, n_e. The stability of different magnetic ground states in the Kondo lattice limit was recently discussed by Doradziński and Spałek (DS) [5]. The DS phase diagram,

[3] Author to whom any correspondence should be addressed.

constructed on the V–n_e plane, has been shown to provide a good qualitative account of the experimental results obtained, e.g., for a series of CeTM (T = Rh, Ni, Rh, Pd; M = Sn, Sb) intermetallics [6]. The existence of inhomogeneous magnetic states (e.g., spin-glass or cluster-glass states) is also possible, however their theoretical interpretation is much more complicated, and usually not considered in simple models of Kondo lattices.

Recently, the ternary compounds REAgAl (RE = La, Ce, Pr, Nd, Tb, Er) have been reported to exhibit spin-glass properties due to structural disorder of Ag and Al atoms, randomly occupying the same crystallographic site in an orthorhombic unit cell of the $CeCu_2$-type [7]. The case of CeAgAl seems most tempting, because of the possible Kondo screening effect of the magnetic moments carried by Ce atoms, which may accompany spin-freezing phenomenon. As all the Ce atoms in this compound occupy a periodic lattice, CeAgAl might be another representative of so-called non-magnetic atom disorder (NMAD) spin glasses, which sometimes exhibit false indications of HF behavior [8]. To address this problem we performed magnetization, magnetic susceptibility, heat capacity, and electrical resistivity measurements on high-quality polycrystalline sample of CeAgAl, and compared the experimental results with the calculated electronic structure of the compound. Moreover, x-ray photoelectron spectroscopy (XPS) studies were carried out to analyze the valence state of the Ce ions in CeAgAl and the hybridization strength between the Ce 4f states and the conduction band. The valence band (VB) electronic states determined by XPS were compared with the *ab initio* density of states calculations. Our results suggest that CeAgAl is a Kondo lattice ferromagnet. We attempt to interpret the ground state properties of this compound with the Doradziński–Spałek approach.

2. Experimental details

A polycrystalline sample of CeAgAl was prepared by arc melting the constituent elements on a water-cooled copper hearth in a high-purity argon atmosphere using an Al getter. The button was remelted several times to promote homogeneity and subsequently annealed in vacuum at 800 °C for 3 weeks. The quality of the obtained material was checked by x-ray powder diffraction on a Siemens D5000 powder diffractometer with Cu Kα radiation. The x-ray diffraction intensities were analyzed using the Powder-Cell 2.4 program. The x-ray pattern was entirely indexed within an orthorhombic unit cell of the $CeCu_2$-type with a statistical distribution of Ag and Al atoms over the Cu site. The refined lattice parameters $a = 4.706$ Å, $b = 7.516$ Å and $c = 7.942$ Å are close to those reported in the literature [9].

DC magnetic measurements were carried out in the temperature range from 1.72 to 300 K in applied magnetic fields up to 50 kOe using a Quantum Design superconducting quantum interference device (SQUID) magnetometer. The AC magnetic susceptibility was measured over the 1.9–300 K interval employing a Lake Shore magnetic susceptometer. The amplitude of the excitation field was 10 Oe at a fixed frequency of 10 kHz.

Electrical resistivity measurements were made using a standard four-probe DC technique. The voltage and current electrical contacts were made by spark welding and silver paste, respectively. The specific heat was measured in the temperature range 300 mK–20 K and in external magnetic fields up to 80 kOe using a Quantum Design PPMS platform.

The x-ray photoelectron spectroscopy (XPS) studies were made at room temperature with monochromatized Al Kα radiation using a PHI-5700 ESCA spectrometer. The sample was scraped with a diamond file under high vacuum immediately before recording a spectrum.

3. Computational methods

In CeAgAl compound (space group $Imma$) Ag and Al atoms are statistically distributed at the crystallographic positions 8h. Later on we argue that the ground state physical properties of CeAgAl are strongly determined by the random distribution of the *non-magnetic* atoms in the atomic sites 8h. In this work the local ordering is an important feature of the modeling of the physical properties of CeAgAl. The coherent potential approximation (CPA) approach is of a single site character and assumes perfect atomic disorder. In CPA calculations no special local atomic configurations is distinguished, therefore this method does not allow one to take the atomic clusterization effect and cannot take into account the local short-range order, which is essential for our modeling. Therefore, the electronic structure of CeAgAl was calculated using tight binding linearized muffin-tin orbitals (TB-LMTO) [10, 11] and full potential linear augmented plane waves (FP-LAPW) methods [13], considering different types of atomic configurations at 8h sites. The calculations were scalar relativistic and spin polarized. The input lattice parameters were equal to those determined from the x-ray diffraction experiment (see section 2).

The TB-LMTO calculations were made employing the atomic sphere approximation (ASA) for the crystal potential [10] with overlapping Wigner–Seitz (WS) spheres centered at the atomic positions. The values of the WS sphere radii were determined in such a way that the sum of all the atomic sphere volumes was equal to the unit cell volume. The exchange–correlation potential (XC) was used in the form proposed by Barth–Hedin [14] with gradient corrections of the Langreth–Mehl–Hu-type [15]. The calculations were performed for 3212 $\vec{k}$ points in the irreducible wedge of the Brillouin zone (BZ), with a total energy error less then 0.01 mRyd. Downfolding was used for 6p Ce and 3d Al states.

In order to estimate the effect of ASA, the FP-LAPW calculations [12] were performed using the Wien2K6 package [13] with the General Gradient Approximation [16] implemented to account for electronic correlations. Muffin-tin spheres with radii 2.50, 2.50 and 2.32 Å were assumed for Ce, Ag, and Al atoms, respectively.

The valence bands were calculated from the partial density of states. The DOS data with different l-symmetry were multiplied by the respective cross sections [17] and convolved with 0.4 eV Lorentzians.

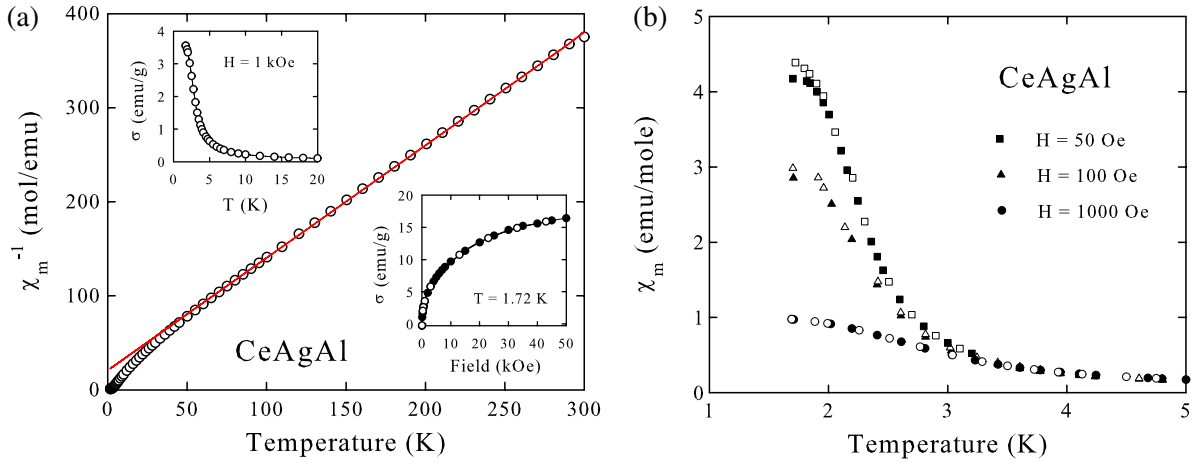

Figure 1. (a) Temperature dependence of the inverse molar magnetic susceptibility of CeAgAl. The solid line is the Curie–Weiss fit with the parameters given in the text. The upper inset shows the low-temperature magnetization measured in a field of 1 kOe. The lower inset displays the magnetization measured at 1.72 K as a function of magnetic field with increasing (full circles) and decreasing (open circles) field strength. (b) Temperature variations of the molar magnetic susceptibility of CeAgAl taken in three different magnetic fields upon cooling the specimen in zero (full symbols) and applied (open symbols) magnetic field.

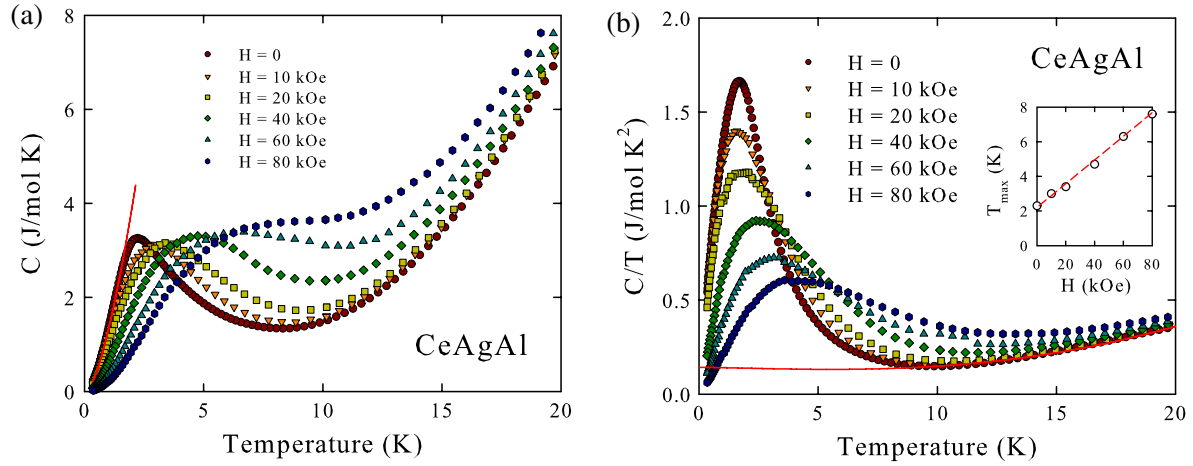

Figure 2. (a) Temperature dependencies of the specific heat of CeAgAl measured in several different magnetic fields. The solid line is a fit of the zero-field data according to the formula given in the text. (b) The same data in the C/T versus T representation. The solid line is the fit described in the text. The inset presents the field variation of the temperature at which the specific heat reaches a maximum. The dashed line emphasizes the proportionality $T_{max} \sim H$.

4. Results and discussion

4.1. Physical properties

The magnetic behavior of CeAgAl is summarized in figure 1. The inverse magnetic susceptibility, displayed in panel a, is proportional to temperature above about 50 K. A least-squares fit of the $\chi(T)$ data to the Curie–Weiss law $\chi(T) = C/(T-\theta)$, where $C = N_A\mu_{eff}^2/3k_B$, N_A is the Avogadro's number, μ_{eff} is the effective magnetic moment, and θ is the paramagnetic Curie temperature, yields the parameters $\mu_{eff} = 2.65\ \mu_B$ and $\theta = -18$ K. The value of μ_{eff} is close to that expected for a free Ce^{3+} ion within the Russel–Saunders coupling scheme. The negative paramagnetic Curie temperature may be indicative of antiferromagnetic correlations, yet its magnitude also suggests the presence of Kondo-type interactions. From the value of θ the characteristic temperature T_K may be estimated to be about 5 K [18]. Below ∼3 K the magnetic susceptibility is strongly field-dependent and exhibits a faint maximum at the lowest temperatures (see figure 1(b)). Moreover, the curves measured in very weak magnetic fields exhibit some irreversibility when taken in zero-field-cooled and field-cooled regimes, similar to that observed for spin frozen Kondo lattice compound $CeCuSi_2$ [19] or Ce_2Agln_3 [20]. This behavior may also suggest weak ferromagnetism below $T_C \cong 2.8$ K, as defined by the inflection point in $\chi(T)$. As shown in the lower inset to figure 1(a), the isothermal magnetization curve $\sigma(H)$, measured up to 50 kOe at 1.7 K, although being strongly curvilinear does not reveal any hysteresis nor remanence effect. The saturation magnetic moment μ_s, obtained from an extrapolation of the σ versus $1/H$ plot to $1/H \to 0$, is equal to 0.94 μ_B.

The results of specific heat measurements performed in several applied magnetic fields between 0 and 80 kOe are

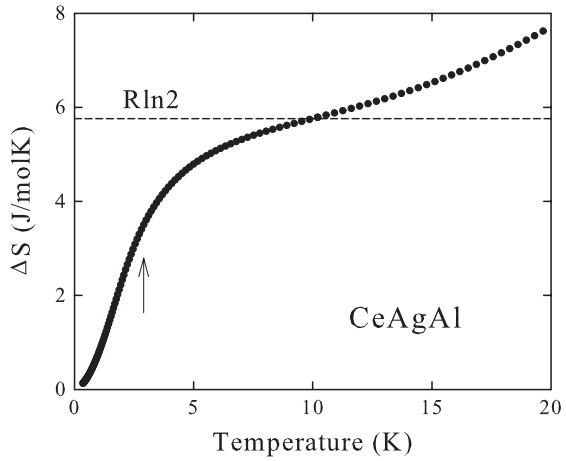

Figure 3. Temperature variation of entropy after subtracting the phonon contribution. The arrow indicates the ordering temperature T_C.

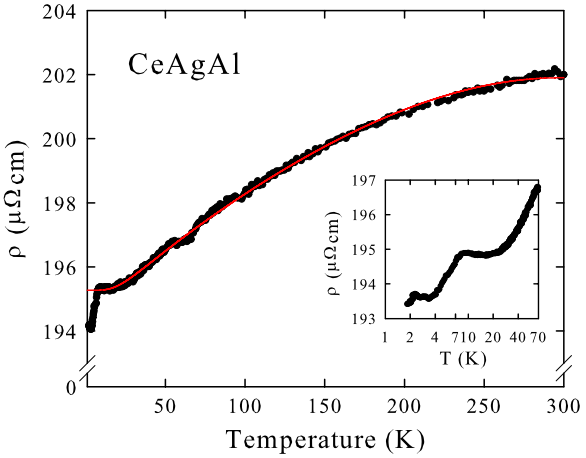

Figure 4. Temperature dependence of the electrical resistivity of CeAgAl. The solid line is the BGM fit discussed in the text. The inset blows up the low-temperature behavior of the resistivity.

shown in figure 2(a) in the form of C versus T and in figure 2(b) as C/T versus T. The $C(T)$ curve is dominated by a broad peak with pronounced tail on the high-temperature side, located at $T_{max} = 2.3$ K in zero field. This anomaly has a shape characteristic of Kondo systems [21–23] and its position agrees well with the prediction $T_{max} = 0.45T_K$ [24], where T_K of about 5 K is assumed, as derived from the magnetic data. However, the maximum cannot be due to the Kondo effect alone because its magnitude is twice as large as that predicted by the $S = 1/2$ Kondo model [25]. In order to account for hump in the specific heat one may consider the crystalline electric field (CEF) effect. However, inspection of the Schottky specific heat with the CEF-level scheme composed of the first and second excited doublets lying at $\Delta_1 \approx 100$ K and $\Delta_2 \approx 140$ K above the doublet ground state (like in similar compounds, e.g., CeRhAl [26]) gave negligible contribution below 10 K. Thus, most likely, the maximum in $C(T)$ arises in CeAgAl because of the onset of the magnetic state. Actually, the low-temperature tail of this peak can be described quite accurately by an expression appropriate for an anisotropic ferromagnet with a gap δ in the magnon dispersion: $C(T) = \gamma T + AT^{3/2}\exp(-\delta/T)$ [27]. The least-squares fit of this expression to the experimental data (the phonon contribution was assumed to be negligible at such low temperatures), shown in figure 2(a), yielded the parameters: $\gamma \approx 210$ mJ mol^{-1} K^{-2}, $A = 1.42$ J mol^{-1} K^{-1}, and $\delta = 0.27$ K. The specific heat peak magnitude at T_C is about 3 J mol^{-1} K^{-1}, i.e. it is strongly reduced in comparison to the value of 12.48 J mol^{-1} K^{-1} corresponding to a crystal electric field doublet ground state. This reduction should be attributed to the Kondo effect [23].

Upon applying magnetic field, the maximum in $C(T)$ diminishes slightly and shifts almost linearly to higher temperatures with rising field strength (see the inset to figure 2(b)). Though smearing of the specific heat peak in magnetic fields, accompanied with some decrease in its magnitude, was also established for archetypal spin glasses like CuMn alloys [28], in the case of CeAgAl the tendency in $C(T)$ changes in fields stronger than 40 kOe and some increase in the magnitude of the maximum is seen, which clearly manifests the Kondo nature of the compound studied.

Above the maximum the C/T data do not follow a T^{-2} dependence, however it may be well described in the range $9.5 \leqslant T < 20$ K by the relationship $C/T = \gamma^\star + \delta T^2 \ln(T/T^\star)$ (see figure 2(b))), which represents a spin-fluctuation contribution $T^3\ln(T/T^\star)$ to the specific heat [29], presumably occurring due to Ce 3d states. The least-squares derived linear coefficient of the specific heat enhanced by the mass-enhancement factor $m^\star/m_0$ here is $\gamma^\star = 142$ mJ mol^{-1} K^{-2}, and the spin-fluctuation temperature amounts to $T^\star = 9$ K.

Figure 3 presents the magnetic entropy $\Delta S = \int_0^T (\Delta C/T)\,\mathrm{d}T$ calculated from the magnetic contribution to the specific heat, derived as $\Delta C = C - C_{ph} \equiv C(\mathrm{CeAgAl}) - C(\mathrm{LaAgAl})$. The entropy at T_{max} is about 2.56 J mol^{-1} K^{-1} and that released at $T_C = 2.8$ K (T_C derived from the magnetic data coincides with an inflection point above the maximum on the $C(T)$ curve) is about 3.53 J mol^{-1} K^{-1}, which means 43% and ∼60 %, respectively, of the value $R\ln 2 = 5.76$ J mol^{-1} K^{-1} that corresponds to the doublet ground state. This distinct entropy reduction comes from the Kondo interactions. Within a simple two level model with an energy splitting of $k_B T_K$ the magnetic entropy of a Kondo system is related to the ratio T_K/T_C in the following manner [22].

$$\Delta S/R = \ln[1 + \exp(-T_K/T_C)] + \frac{T_K}{T_C}\frac{\exp(-T_K/T_C)}{1 + \exp(-T_K/T_C)}.$$

The Kondo temperature T_K estimated from this relation is 5.1 K, i.e. nearly same as that derived from the magnetic susceptibility data. Moreover, according to the $S = 1/2$ Kondo model [25], this value of T_K implies that a Kondo maximum in the specific heat occurs at $T_{max} = 0.45T_K = 2.3$ K in perfect agreement with the experimental findings. In a high magnetic field of 8 T the magnetic entropy released at T_{max} rises to ∼50 % of Rln2. This behavior is in line with theoretical predictions for Kondo systems [24] and numerous experimental results (e.g., [21, 23]).

Figure 4 presents the temperature dependence of the resistivity of CeAgAl. It shows a metallic behavior, however

Table 1. Atomic positions 4e and 8h in the unit cell of CeAgAl, considered in the LMTO and LAPW calculations performed for different atomic ordering models (1–4). The calculations were carried out for different occupations of the 8h positions by Ag and Al atoms (see the text). The assumed experimental lattice parameters were: $a = 4.706$ Å, $b = 7.516$ Å, and $c = 7.942$ Å.

x, y, z	(1)	(2)	(2)	(4)
0.5, 0.25, 0.5377	Ce	Ce	Ce	Ce
0.5, 0.75, 0.4623	Ce	Ce	Ce	Ce
0, 0.75, 0.0377	Ce	Ce	Ce	Ce
0, 0.25, 0.9623	Ce	Ce	Ce	Ce
0.5, 0.551, 0.8354	Ag	Al	Ag	Al
0.5, 0.449, 0.1646	Ag	Al	Ag	Al
0, 0.449, 0.3354	Ag	Al	Al	Ag
0, 0.551, 0.6646	Ag	Al	Al	Ag
0.5, 0.949, 0.8354	Al	Ag	Ag	Al
0.5, 0.051, 0.1646	Al	Ag	Ag	Al
0, 0.051, 0.3354	Al	Ag	Al	Ag
0, 0.949, 0.6646	Al	Ag	Al	Ag

the absolute values of the resistivity are rather large and their temperature dependence is very weak (the ratio between the resistivity measured at room temperature and 2 K is only 1.03), both these features being characteristic of scattering on structural disorder. Above 8 K the $\rho(T)$ curve can be well approximated by the Bloch–Grüneisen–Mott formula [30]

$$\rho(T) = \rho_0 + 4RT\left(\frac{T}{\Theta_D}\right)^4 \int_0^{\frac{\Theta_D}{T}} \frac{x^5 dx}{(e^x - 1)(1 - e^{-x})} - KT^3$$

where ρ_0 is the residual resistivity, Θ_D stands for the Debye temperature and R is a constant, whereas the cubic term KT^3 describes interband scattering processes. Fitting the above expression to the experimental data of CeAgAl (note the solid line in figure 4) yielded the parameters: $\rho_0 = 195$ $\mu\Omega$ cm, $R = 0.034$ $\mu\Omega$ cm K^{-1}, $K = 1.29 \times 10^{-7}$ $\mu\Omega$ cm K^{-3} and $\Theta_D = 123$ K.

At $T \approx 2.8$ K the resistivity shows a rapid drop due to the onset of long-range ferromagnetic ordering (see the inset to figure 4). The shallow minimum on the $\rho(T)$ curve observed at about 16 K, followed by a weak maximum ρ_{max} centered around 9.5 K, are reminiscent of the behavior of dense Kondo systems with a coherence temperature corresponding to the position of ρ_{max}. In most of the Ce intermetallics the coherence effect is observed at higher temperatures, however, the coherence temperature can be small if the hybridization of the 4f states with the conduction electrons is weak, as is the case for CeAgAl. Using the standard expression for the virtual bound state width [32] one obtains that $k_B T_{max} \sim \pi V^2 \mathrm{DOS}(\varepsilon_F)$, where V is the magnitude of intra-atomic hybridization of f states with the conduction electrons. With typical values $\mathrm{DOS}(\varepsilon_F) \sim 1/3$ (eV atom)$^{-1}$ and $V \sim 40$ meV (see section IVB), $T_{max} \sim 20$ K can be derived, which is roughly consistent with the experimental observation.

4.2. Electronic structure

According to the literature data [9], the crystallographic unit cell of CeAgAl (space group *Imma*) contains Ce atoms at the positions 4e, and Ag and Al atoms are statistically distributed over the positions 8h. Nevertheless, in the LMTO and LAPW calculations we have considered four different types of atomic arrangement of the atoms at the 8h sites presented in table 1,which form a primitive space group from the base orthorhombic *Imma* space group of the $CeCu_2$-type.

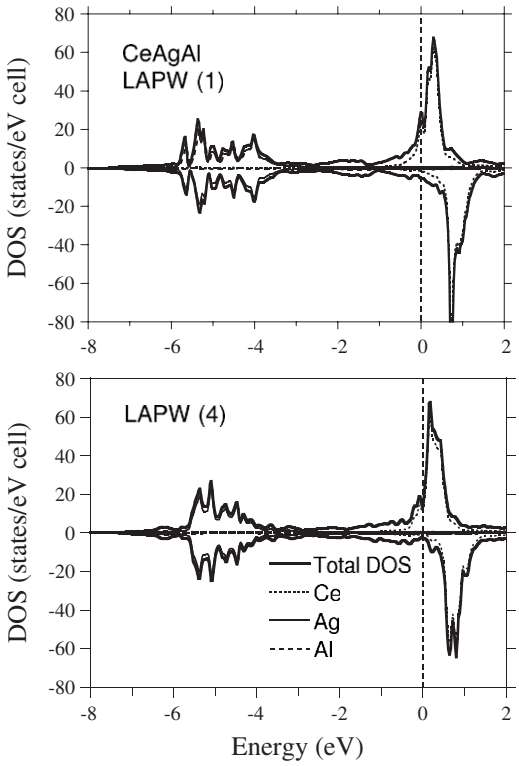

Figure 5. The total and partial density of states obtained for CeAgAl from the LAPW calculations performed for models (1) and (4), described in the text.

In figure 5 we compare the density of states in CeAgAl calculated by the LAPW method for the two different Ag–Al configurations considered. Models (1) or (2) and (3) or (4), respectively gave very similar results of magnetic state with the magnetic moment of Ce atoms being about 0.9 μ_B. In the vicinity of the Fermi energy the main contribution to DOS comes from 4f states of cerium. The calculations predicted a pseudogap in the minority spin direction at ϵ_F, whereas for the majority spin direction the f states form a local maximum in DOS, which is responsible for the magnetic moment formation on cerium atoms. As is apparent from figure 5, a band located in the binding energy range of ∼4–7 eV originates mainly from the d states of Ag.

Similar results were obtained via the LMTO method, as exemplified for model (1) and (3) in figure 6. Shown in this figure are the partial DOSs calculated for particular contributions with different l-symmetry. Clearly, the bands near ϵ_F are composed of the Ce f and d states hybridized with the p states of Ag and Al. The magnetic moments derived from the LMTO calculations are of about 0.6 μ_B for models (1) and (2) and 0.17 μ_B for the atomic arrangement described by model (3) or (4).

Further information on the hybridization effect between cerium and ligand states may be derived from the analysis of

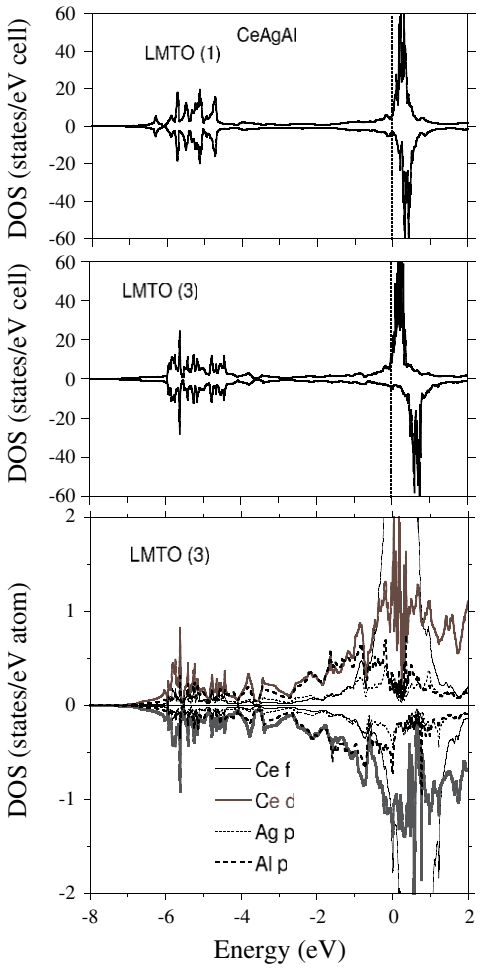

Figure 6. Comparison of the density of states in CeAgAl calculated within the LMTO approach for two different Ag–Al configurations denoted in the text as models (1) and (3). The bottom panel shows the partial DOS derived for model (3).

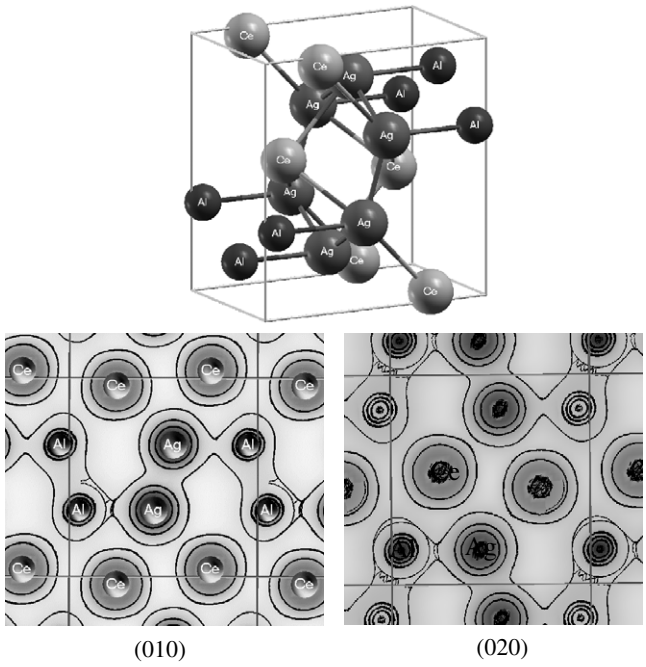

Figure 7. Total valence charge densities in CeAgAl calculated by the LAPW method within the GGA approximation for the planes (010) and (020) assuming model (1) for the atoms distribution. The unit cell considered is shown.

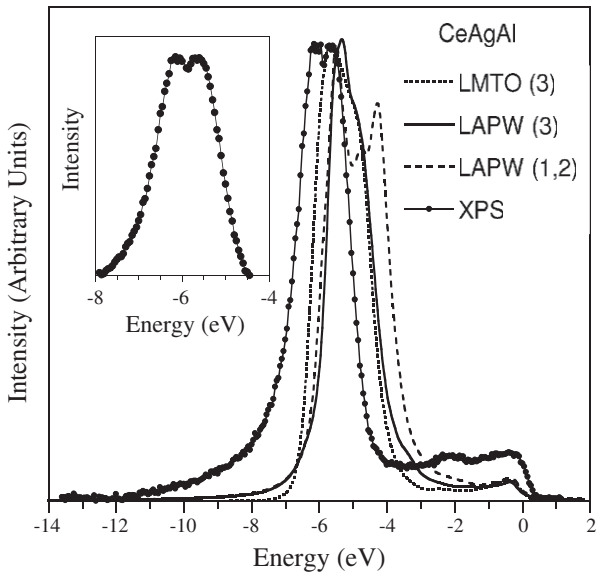

Figure 8. Experimental valence band spectrum (corrected by background) of CeAgAl (full circles) compared with the results of the LMTO and LAPW calculations (solid, dashed and dotted lines) performed for models (1), (2) and (3), as described in the text. The calculated spectra were convolved with Lorentzians of half-width 0.4 eV, taking into account proper cross sections for bands with different l symmetry. For clarity the spectrum is shown also in the inset.

the total valence charge densities, displayed in figure 7. The results presented in the figure were obtained by the LAPW calculations within the GGA approximation performed for the Ag–Al atomic ordering (1) within the 8h sites. The maps presented in the figure show that the charge bonding between Ce and Ag atoms is stronger than the bonding between Ce and Al atoms. As a result, the charge distribution at the Ce positions is strongly dependent on the atomic ordering. In consequence, it strongly influences the magnetic interactions between Ce ions.

Figure 8 shows the experimental XPS valence band spectrum corrected for background. It is composed of two clearly separated parts. The experimental data are compared with the calculated XPS spectra derived via the LMTO and LAPW methods for the different structural models considered. The theoretical spectra were obtained from the partial densities of states convolved with a Lorentzian with a 0.4 eV half-width to account for the instrumental resolution and multiplied by the corresponding cross sections for the partial states of Ce, Ag, and Al with different l-symmetry, taken from [17]. Qualitatively, the best agreement between the XPS spectra obtained experimentally and the calculated ones is observed for model (3), which reproduces the double-peak nature of the VB spectrum (see figure 8). One may conclude, that the XPS VB spectrum is not described well enough by the crystallographic models considered and the distribution of the Ag and Al atoms in positions 8h are random.

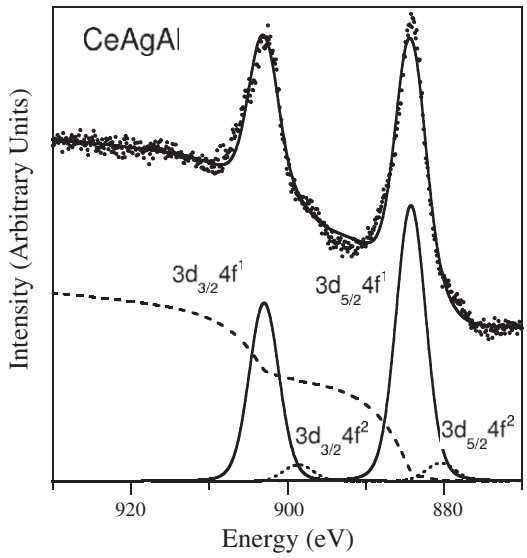

Figure 9. Ce 3d XPS spectra deconvolved for $3d4f^1$ and $3d4f^2$ lines with the spin–orbit splitting of 18.6 eV.

Shown in figure 9 are plots of the Ce 3d core-level XPS spectra. The main components $3d^9_{5/2}4f^1$ and $3d^9_{3/2}4f^1$ exhibit a spin–orbit splitting $\Delta_{SO} = 18.6$ eV. The appearance of the $3d^94f^2$ components is a clear manifestation of the intra-atomic hybridization between the 4f electrons and conduction band. From the analysis of these spectra according to the Gunnarsson and Schönhammer (GS) approach [31] (for details on the procedure see also [26]) one obtains a hybridization energy Δ of about 40 meV, with an accuracy of the order of 15%. The parameter Δ accounts for the hybridization part of the Anderson Hamiltonian [32] and it is defined as $\pi V^2 N(\epsilon_F)$, where $N(\epsilon_F)$ is the density of states at the Fermi level and V stands for the hybridization matrix element. Within the approximations inherent to the GS theory some error in the determination of the hybridization strength is due to uncertainty in the intensity ratio $3d^9f^1$:$3d^9f^2$, directly related to the accuracy of decomposition of the spectrum, as well as to proper background subtraction. It is worthwhile noting that in the 3d XPS spectrum of CeAgAl no sizable $3d^9f^0$ contributions are observed (see figure 9), which implies that all the Ce ions in this compound are in the stable trivalent state. Moreover, the rather small hybridization effect inferred from the XPS data is in line with the results of the afore-discussed electronic structure calculations.

5. Summary

The orthorhombic compound CeAgAl appears to be a Kondo lattice that orders ferromagnetically below $T_C = 2.9$ K. The characteristic energy scales are given by the coherence temperature $T_C \approx 10$ K and the Kondo temperature $T_K \approx 5$ K. The core-level 3d Ce XPS spectra have revealed a stable configuration of the 4f shell and a rather weak intrasite hybridization effect, which is also well supported by the *ab initio* calculations. The simple band structure calculations have yielded a magnetic ground state with a calculated magnetic moment close to that observed experimentally. The best agreement between the calculated and measured valence band XPS spectra was obtained for structure models in which Ag and Al atoms have a tendency to randomly occupy the same crystallographic site in an orthorhombic unit cell. This randomness changes the local charge density on Ce atoms and in consequence the exchange interactions between the Ce atoms depend on the local surrounding, as characteristic of non-magnetic atom disorder (NMAD) systems. As a result a spin-glass ground state in CeAgAl would also be possible. The co-existence of long-range order and a spin-glass state was reported in the series of RAgAl compounds, where R is rare-earth element [7]. In most of the magnetically ordered RAgAl systems the postulated spin-glass state is NMAD driven, due to the random distribution of the non-magnetic atoms. Actually, the specific heat data of CeAgAl could also be discussed on the base of spin-glass-type behavior. For canonical spin-glass systems one expects a broad maximum in $C(T)$ to occur at a temperature $T_{max} \sim 1.4T_f$ and a power law dependence $C \sim T^{3/2}$ for $T > T_{max}$ (see [33]). Though such a behavior is indeed observed for CeAgAl, the magnetic and electrical transport properties of this compound seem to rule out the spin-glass scenario.

Formation of the magnetic ground state in CeAgAl could be analyzed on the basis on the Doradziński and Spałek (DS) model [5]. In this approach the stability of the paramagnetic versus the magnetic ground state in the Kondo lattice limit depends on the on-site hybridization energy V between the f electrons and the conduction electrons and on the total number of electrons per atom $n_e = n_c + n_f$, where n_c is the number of conduction electrons and n_f is the occupation number of the f shell. Generally, the DS diagram reasonably describes the ground state properties of the series of ternary compounds [6]. The microscopic parameters V and n_f can be determined experimentally from the x-ray photoemission spectra using the Gunnarsson–Schönhammer approach, which is based on the Anderson-impurity model [31, 26]. For CeAgAl a very crude estimate gives $n_c < 0.8$, while from the XPS spectra one derives $n_f \sim 1$ and $V = (\Delta/(\pi N(\epsilon_F)))^{1/2} \approx 55$ meV. With these parameters the compound is located on the V–n_e plane in the DS diagram in the ferromagnetic region, very near the line of separation of the ferromagnetic and antiferromagnetic phases. To account for such effects more sophisticated theories should be formulated. Another important finding is that according to the DS diagram CeAgAl is located quite away from the border between magnetic metallic and Kondo-insulating ground states. Thus, the magnetic state in this compound is rather stable and critical behavior at magnetic instability is unlikely to be achieved under external pressures of easily accessible magnitudes.

Acknowledgments

This work was part of the research program of the National Scientific Network ‘Materials with strongly correlated electrons’. The authors acknowledge financial support from Grants No: 1 P03B 052 28, 1 P03B 094 30, N202 038 31/1805 and N202 116 32/3270 of the Polish Ministry of Science and

Higher Education. The authors thank Józef Deniszczyk for discussion.

References

[1] Stewart G R 1984 *Rev. Mod. Phys.* **56** 755
[2] Greve N and Steglich F 1991 Heavy Fermions *Handbook on the Physics and Chemistry of Rare Earths* vol 14, ed K A Gschneidner Jr and L Eyring (Amsterdam: North-Holland) p 343
[3] Steglich F, Geibel C, Gloos K, Olesch G, Schank C, Wassilew C, Loidl A, Krimmel A and Stewart G R 1994 *J. Low Temp. Phys.* **95** 3
[4] Doniach S 1977 *Physica* B **91** 231
Jullien R, Fields J N and Doniach S 1977 *Phys. Rev.* B **16** 4889
Jullien R, Fields J and Doniach S 1977 *Phys. Rev. Lett.* **38** 1500
Lacroix C and Cyrot M 1979 *Phys. Rev.* B **20** 1969
[5] Doradziński R and Spałek J 1997 *Phys. Rev.* B **56** R14239
Doradziński R and Spałek J 1998 *Phys. Rev.* B **58** 3293
[6] Ślebarski A 2006 *J. Alloys Compounds* **423** 15
[7] Suresh K G, Dhar S K and Nigam A K 2005 *J. Magn. Magn. Mater.* **288** 452
[8] Gschneider K A Jr, Tang J, Dhar S D and Goldman A 1990 *Physica* B **163** 507
[9] Fornasini M L, Iandelli A, Merlo F and Pani M 2000 *Intermetallics* **8** 239
[10] Andersen O K and Jepsen O 1977 *Physica* B **91** 317
[11] Andersen O K and Jepsen O 1984 *Phys. Rev. Lett.* **53** 2571
[12] Singh D J 1994 *Planewaves, Pseudopotentials and the LAPW-method* (Boston, MA: Kluwer–Academic)
[13] Blaha P, Schwarz K, Madsen G, Kvasnicka D and Luitz J 2001 *WIEN2k, An Augmented Plane Wave + Local Orbitals Program for Calculating Crystal Properties* Karlheinz Schwarz, Techn. Universitat Wien, Austria
[14] von Barth U and Hedin L 1972 *J. Phys. C: Solid State Phys.* **5** 1629
[15] Hu C D and Langreth D C 1985 *Phys. Scr.* **32** 391
[16] Perdew J P, Burke K and Ernzerhof M 1996 *Phys. Rev. Lett.* **77** 3865
[17] Yeh J J and Lindau I 1985 *At. Data Nucl. Data Tables* **32** 1
[18] Hewson A C 1993 *The Kondo Problem to Heavy Fermions* (Cambridge: Cambridge University Press)
[19] Nishioka T, Tabata Y, Taniguchi T and Miyako Y 2000 *J. Phys. Soc. Japan* **69** 1012
[20] Lu J J, Lu Y M, Lee M K, Mo T S and Jang L Y 2006 *J. Magn. Magn. Mater.* **305** 259
[21] Bader S D, Phillips N E, Maple M B and Luengo C A 1975 *Solid State Commun.* **16** 1263
[22] Yashima H, Mori H, Sato N, Satoh T and Kohn K 1983 *J. Magn. Magn. Mater.* **31–34** 411
[23] Bredl C D, Steglich F and Schotte K D 1978 *Z. Phys.* B **29** 327
[24] Schotte K D and Schotte U 1975 *Phys. Lett.* A **55** 38
[25] Desgranges H-U and Schotte K D 1982 *Phys. Lett.* A **91** 240
[26] Ślebarski A, Goraus J, Jezierski A and Zygmunt A 2004 *Phys. Rev.* B **70** 235112
[27] Sereni J 1991 *Handbook on the Physics and Chemistry of Rare Earths* vol 15, ed K A Gschneidner Jr and L Eyring (New York: Elsevier Science) p 1
[28] Brodale G E, Fisher R A, Fogle W E, Phillips N E and van Curen J 1984 *J. Magn. Magn. Mater.* **31–34** 1331
[29] Doniach S and Engelsberg S 1966 *Phys. Rev. Lett.* **17** 750
[30] Mott N F and Jones H 1958 *The Theory of the Properties of Metals and Alloys* (Oxford: Oxford University Press) p 240
[31] Gunnarsson O and Schönhammer K 1983 *Phys. Rev.* B **28** 4315
Fuggl J C, Hillebrecht F U, Zolnierek Z, Lässer R, Freiburg Ch, Gunnarsson O and Schönhammer K 1983 *Phys. Rev.* B **27** 7330
[32] Anderson P W 1961 *Phys. Rev.* **124** 41
[33] Mydosh J A 1993 *Spin Glasses: An Experimental Introduction* (London: Taylor and Francis)